Post-deposition Processing Methods To Induce Preferential Orientation in Contorted Hexabenzocoronene Thin Films

Anna M. Hiszpanski,[†] Stephanie S. Lee,[†] He Wang,[†] Arthur R. Woll,[‡] Colin Nuckolls,[§] and Yueh-Lin Loo[†,*]

[†]Department of Chemical and Biological Engineering, Princeton University, Princeton, New Jersey 08544, United States, [‡]Cornell High Energy Synchrotron Source, Cornell University, Ithaca, New York 14853, United States, and [§]Department of Chemistry, Columbia University, New York, New York 10027, United States

ABSTRACT The structuring in organic electrically active thin films critically influences the performance of devices comprising them. Controlling film structure, however, remains challenging and generally requires stringent deposition conditions or modification of the substrate. To this end, we have developed post-deposition processing methods that are decoupled from the initial deposition conditions to induce different out-of-plane molecular orientations in contorted hexabenzocoronene (HBC) thin films. As-deposited HBC thin films lack any long-range order; subjecting them to post-deposition processing, such as hexanes-vapor annealing, thermal annealing, and physical contact with elastomeric poly(dimethyl siloxane), induces crystallization with increasing extents of preferential edge-on orientation, corresponding to greater degrees of in-plane π-stacking. Accordingly, transistors comprising HBC thin films that have been processed under these conditions exhibit field-effect mobilities that increase by as much as 2 orders of magnitude with increasing extents of molecular orientation. The ability to decouple HBC deposition from its subsequent structuring through post-deposition processing affords us the unique opportunity to tune competing molecule–molecule and molecule–solvent interactions, which ultimately leads to control over the structure and electrical function of HBC films.

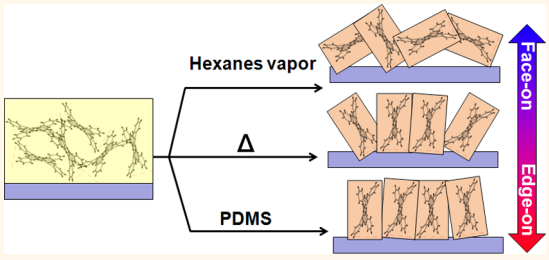

KEYWORDS: preferential molecular orientation · contorted hexabenzocoronene · post-deposition processing · organic thin-film transistor

Given that charge transport in organic semiconductors occurs preferentially along the direction of π-stacking, the ability to prescribe preferential molecular orientation within electrically active layers has been a long sought goal to improve the characteristics of organic thin-film transistors (TFTs), single-carrier diodes, and solar cells.[1−3] Several approaches have been explored to control the molecular orientation of organic semiconductor thin films over multiple length scales. Changes to molecular parameters, such as regioregularity, isomerism, and molecular weight; modifications to substrate surfaces through self-assembled monolayer adsorption; and alterations to deposition conditions have all been shown to influence the structure of and overall orientation in organic semiconductor thin films.[4−8] The confinement of organic semiconductors within the pores of alumina oxide templates and the application of external fields and temperature gradients during zone-casting and dip-coating have also been shown to induce preferential orientation over macroscopic length scales.[9,10] Though diverse in approach, these methods share a common trait that competing molecule–substrate, molecule–molecule, and molecule–solvent interactions during deposition dictate the preferential orientation in organic semiconductor thin films. These approaches thus mandate stringent conditions over which the organic semiconductors are deposited.[10,11]

More ideal would be to decouple film formation from structural development, during which post-deposition processing renders additional control over structure. Post-deposition processing has been applied to decouple organic semiconductor deposition from some aspects of its structure development, such as the molecular packing of pentacene, the in-plane crystal orientation of triethylsilylethynyl anthradithiophene

* Address correspondence to lloo@princeton.edu.

Received for review August 30, 2012 and accepted December 10, 2012.

Published online December 10, 2012
10.1021/nn304003u

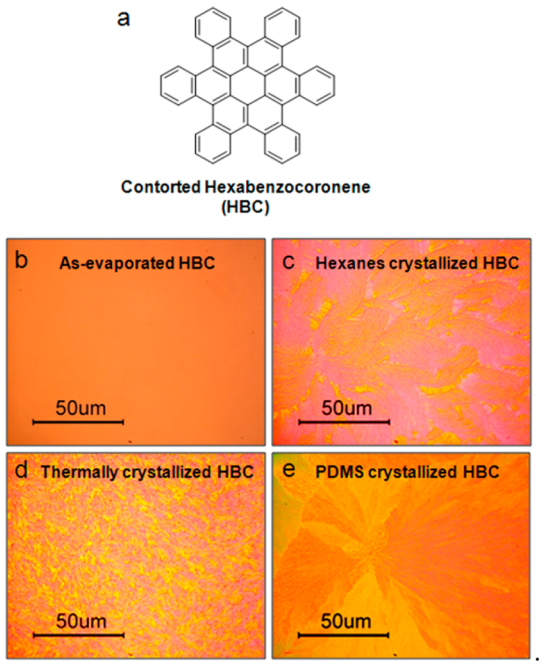

Figure 1. Chemical structure of contorted hexabenzocoronene, HBC (a), and polarized optical micrographs of thermally evaporated thin films of HBC before (b) and after post-deposition treatments (c–e). The contrast in (c–e) was enhanced for clarity.

(TES ADT), and the degree of edge-on orientation of *N*,*N*′-1*H*,1*H*-perfluorobutyl dicyanoperylenecarboxydiimide (PDIF-CN_2).[12−14] In the particular case of PDIF-CN_2, the organic semiconductor adopts a preferential edge-on orientation upon deposition; subsequent processing enhances macroscopic crystallinity and further increases the extent of edge-on orientation. Herein, we begin with an amorphous film exhibiting no preferential molecular orientation, and we demonstrate post-deposition processing methods that permit tuning of the out-of-plane molecular orientation of contorted hexabenzocoronene, HBC (Figure 1a). With different post-deposition processing conditions, we can access orientations ranging from slightly face-on to extremely edge-on, as quantified by the Herman's orientation function, without the need for substrate modification. These approaches are robust and versatile as organic semiconductors can be deposited on a single common substrate and subsequently crystallized with prescribed molecular orientations. We have chosen to work with contorted HBC because of its highly nonplanar geometry, which has been reported to enhance molecular interactions with fullerene derivatives in solar cells.[15,16] Because unsubstituted HBC exhibits limited solubility in common organic solvents, thermal sublimation is the deposition method of choice, yielding films with no long-range order. The fact that HBC forms a largely amorphous film during deposition has allowed us to decouple and control the film's subsequent structural development *via* post-deposition treatments that are independent of the conditions from which the films

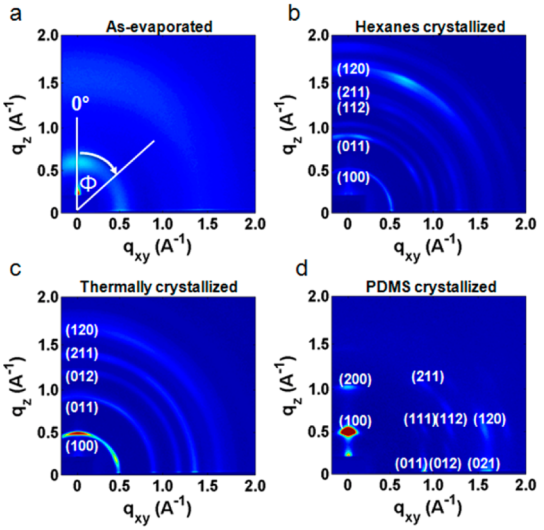

Figure 2. Indexed grazing-incidence X-ray diffraction images of as-evaporated (a), hexanes-vapor annealed (b), thermally annealed (c), and PDMS-crystallized (d) HBC films on HMDS-treated SiO_2. Azimuthal anisotropy of diffracted intensity indicates preferential orientation of HBC.

were initially formed. Subjecting as-evaporated HBC thin films to three post-deposition treatments— hexanes-vapor annealing, thermal annealing, and direct contact with cross-linked poly(dimethyl siloxane), PDMS, elastomeric stamps—all induce large-scale crystallization of the same polymorph but with substantial differences in HBC's preferential out of plane orientation. Not surprisingly, TFTs comprising these electrically active layers exhibit mobilities that are correlated with the extent with which HBC is preferentially oriented edge-on.

RESULTS AND DISCUSSION

As-evaporated HBC films appear featureless on both micrometer (Figure 1b) and nanometer (Figure S1a in Supporting Information) length scales, suggesting a lack of long-range order. Figure 2a contains a grazing-incidence X-ray diffraction (GIXD) image of an as-evaporated HBC film showing modest scattered intensities centered about q = 0.57 and 1.51 Å^{-1}. Given the breadth of the intensity distribution, we attribute the scattered intensity to subnanometer nearest-neighbor correlations.[17] Indeed, near-edge X-ray absorption fine structure spectroscopy, NEXAFS, studies also confirm no preferential molecular orientation in as-evaporated films (Figure S2a). This lack of structure is unusual since small-molecule organic semiconductors—given their tendency to π-stack—readily crystallize during film formation, as in the case of pentacene and hexa-peri-hexabenzocoronene, a planar molecule that shares the same coronene core as HBC.[5,18] The lack of order in as-evaporated HBC films presumably stems from the molecule's peripheral aryl groups, which are bent out of the plane that is defined by the coronene core.[19,20] As a consequence of this contortion, intermolecular $\pi-\pi$ interactions are reduced, frustrating the molecules

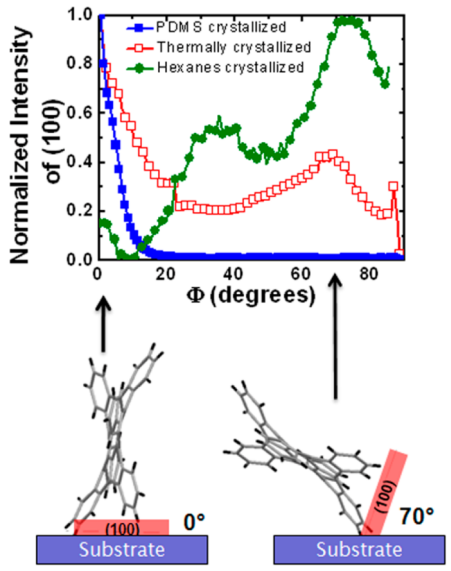

Figure 3. Normalized intensity of the (100) reflection plotted as a function of Φ, the azimuthal angle measured from q_{xy} = 0. Schemes indicate the molecular orientations with respect to the substrate that is inferred from the intensity anisotropy.

and preventing crystallization during deposition. Without any post-deposition treatment, these films remain disordered even after 2 years at ambient conditions.

Optical micrographs illustrating the large-scale structuring of HBC films after they have been subjected to these different post-deposition processing treatments are shown in Figure 1c–e. Although all of these treatments yield micrometer-size spherulites, the detail textures that make up these spherulites vary substantially. Despite HBC being only sparingly soluble, exposure to saturated hexanes vapor induces the formation of spherulites with a "feathery" texture, as seen in Figures 1c and S1b. Annealing HBC with a myriad of other solvent vapors also induces crystallization of HBC, albeit a different polymorph results. We have thus chosen to limit the scope of the work reported herein to hexanes-vapor annealing so we access the same polymorph as thermal annealing and physical contact with PDMS. Thermal annealing induces cold crystallization of HBC below its melting temperature of 516 °C.[21] This process results in a grainier texture (Figure 1d and Figure S1c) when HBC is fully crystallized. Interestingly, contacting as-evaporated HBC with an elastomeric PDMS stamp also induces large-scale crystallization at room temperature (Figure 1e). Equally interesting is the fact that the texture of spherulites resulting from PDMS-induced crystallization is yet different from those of spherulites formed by solvent-vapor and thermal annealing. Instead, these spherulites resemble the superstructures commonly observed in semicrystalline polymer thin films and those more recently reported in solvent-vapor-annealed TES ADT thin films.[22–25] As we show subsequently, such differences in the spherulite texture are strongly correlated with the molecular orientation of HBC in these treated thin films.

That direct contact with PDMS stamps induces large-scale HBC crystallization is surprising. On the basis of NEXAFS experiments conducted in partial electron yield mode at the carbon edge, we know that residual oligomers from the PDMS stamps remain on the surface of HBC films (Figure S3a); we thus speculate that these residual oligomers induce crystallization as the process continues even after the stamp is removed. Furthermore, control experiments involving HBC in contact with Au-coated PDMS reveal no evidence of crystallization. While we cannot rule out that PDMS oligomers are plasticizing HBC, thereby providing a means for structural rearrangement, we hypothesize it is the unfavorable interactions between residual uncrosslinked oligomers introduced at the film surface that causes HBC to densify in order to minimize unlike contact. Consistent with this hypothesis is the fact that PDMS-containing block copolymers exhibit extremely large Flory-Huggins interaction parameter, χ, so these materials microphase separate readily even at low molecular weights.[26] Indeed, NEXAFS studies confirm the presence of oligomers only on the film surface. That no oligomers are detected along the depth of HBC films (Figure S2b) implicates against plasticization. Given that HBC selectively crystallizes in regions of PDMS contact (noncontacted regions do not crystallize), this method also allows us to induce HBC crystallization in arbitrary patterns defined by the features of the PDMS stamp (Figure S4).

Figure 2 shows the indexed GIXD images of untreated and post-deposition treated films. Consistent with the single-crystal structure of HBC, these crystalline thin films all adopt the $P2_1/c$ crystal structure.[19] While the GIXD images in Figure 2b–d share the same reflections, the intensity distribution as a function of the azimuthal angle, Φ, varies dramatically. In particular, we observe reflections whose intensities are distributed across a broad distribution of azimuthal angles in the GIXD images acquired on the hexanes-vapor-annealed and thermally annealed HBC films, whereas we observe azimuthal-angle-specific sharp spots in the GIXD image obtained on the HBC film that had been in contact with PDMS. Such differences in the azimuthal intensity distribution are indicative of variations in the extent of molecular orientation, with the HBC film that had been in contact with PDMS exhibiting a substantially stronger preferential orientation.

Tracking the intensity of a particular reflection as a function of Φ allows us to quantitatively elucidate the ensemble-average molecular orientation of HBC with respect to the substrate in the footprint of the incident beam (1 mm × 5 mm). To quantify the extent of preferential orientation, we analyzed the intensity distribution of the (100) reflection, corresponding to the planes that are perpendicular to the coronene core. Figure 3 shows the normalized intensity of the (100) reflection plotted as a function of Φ. Intensities centered

around $\Phi = 0°$ correspond to (100) planes stacked preferentially out-of-plane, or equivalently, HBC preferentially adopting an edge-on orientation, as depicted by the left cartoon in the inset of Figure 3; scattered intensities at $\Phi = 90°$ correspond to HBC preferentially adopting a face-on orientation.

The intensity distribution of the (100) reflection derived from the GIXD image of the hexanes-vapor-annealed film (filled circles in Figure 3) is broad and spans the entire range of azimuthal angles sampled, indicating that HBC adopts a correspondingly broad distribution of molecular orientation. An enhancement in the intensity distribution around $\Phi = 75°$, however, suggests that hexanes-vapor-treated HBC films exhibit a slight preference for face-on orientation, in which π-stacking is normal to the substrate. The intensity distribution of the (100) reflection for the thermally annealed HBC film is shown as unfilled rectangles in Figure 3. As with the intensity distribution of the hexanes-vapor-annealed HBC film, the intensity associated with the (100) reflection of the GIXD image of the thermally annealed HBC film is also broadly distributed across all azimuthal angles. We observe, however, an enhancement in intensity about $\Phi = 0°$, corresponding to HBC adopting a slight preference for an edge-on orientation. Though thermal annealing and solvent-vapor annealing are two common post-deposition processing methods employed to induce crystallization in organic semiconductor thin films, these methods have not—until now—provided differentiation in molecular orientation.[22,27] The intensity of the (100) reflection extracted from the GIXD of the PDMS-treated HBC film as a function of azimuthal angle is shown with filled rectangles in Figure 3. We observe that the intensity is highly concentrated around $\Phi = 0°$, indicating that nearly all of the HBC are oriented edge-on with their (100) plane parallel to the substrate. This edge-on molecular orientation is particularly favorable for lateral charge transport in TFTs since π-stacking is now parallel to the substrate.

Previously, modification of substrate surface energy *via* self-assembled monolayer adsorption prior to organic semiconductor deposition was reported to induce differences in the molecular orientation in the active layers.[5−7] Yet, chemical treatments to the organic semiconductor−dielectric surface at which charges transport will necessarily affect the electrical characteristics of TFTs comprising such active layers. Given that our organic semiconductor−dielectric interface is chemically invariant, we are able to systematically evaluate correlations between molecular orientation and HBC's electrical properties in TFTs that had been treated under these different conditions. Figure 4a contains the transfer characteristics of top-contact, bottom-gate TFTs comprising HBC after the active layers had been subjected to the different post-deposition processing treatments ($I-V$ characteristics of representative devices are shown in Figure S5). We extracted mobilities from the saturation regime of the transfer characteristics according to

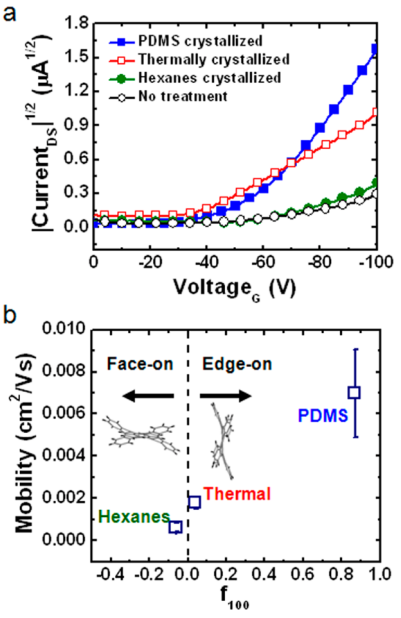

Figure 4. (a) Representative transfer characteristics (V_{sd} held constant at −100 V) from which hole mobilities were extracted from as-evaporated and crystalline HBC thin-film transistors. (b) Hole mobilities, which are scaled by the mobility of thin-film transistors fabricated from untreated HBC films (2.4×10^{-4} cm^2/V·s), plotted as a function of Hermans' orientation function, f_{100}, which quantifies the direction of crystal orientation, and is calculated for the (100) reflection. Error bars represent the standard deviation of mobility from 13 to 18 transistor measurements. The greater variability in the mobilities extracted from the PDMS-treated HBC TFTs likely stems from greater variability in the processing of PDMS-treated films (*i.e.*, the force with which PDMS is peeled from the underlying HBC; the amount of oligomer left on the film surface, *etc.*).

$$I_{DS} = \frac{1}{2}\frac{W}{L}\mu C_{ox}(V_G - V_t)^2 \qquad (1)$$

where the channel width (W) of our transistors was 2000 μm, the channel length (L) was 100 μm, and the capacitance of the 300 nm thick thermal oxide (C_{ox}) was 1.06×10^{-8} F/cm^2. Of 14 TFTs comprising as-evaporated HBC films, the average mobility was $2.4 \pm 0.8 \times 10^{-4}$ cm^2/V·s. These devices also exhibited an unusually large threshold voltage ($V_T = -55 \pm 5$ V) and a correspondingly small on/off ratio of $I_{on}/I_{off} = 30$. Annealing the HBC active channels with hexanes vapor improved the mobility of TFTs by nearly a factor of 3 compared to devices fabricated with untreated films. Of 14 devices tested, the average mobility was $6.2 \pm 1.9 \times 10^{-4}$ cm^2/V·s. The threshold voltage and on/off ratio of these devices, however, did not improve compared to devices with as-evaporated HBC. In the case of devices comprising thermally annealed HBC active channels, in which a slight preference for edge-on orientation is observed, the mobility increased nearly a factor of 2 compared to those comprising hexanes-vapor-crystallized films, and

an order of magnitude higher compared to devices comprising as-evaporated HBC. Of 14 devices tested, the average mobility was $1.8 \pm 0.3 \times 10^{-3}$ $cm^2/V \cdot s$. These devices also exhibited a markedly improved V_T of -27 ± 5 V, with an order of magnitude improvement in on/off ratio. Finally, TFTs fabricated with PDMS-treated films that exhibited a strong preference for edge-on orientation demonstrated mobilities of $7.0 \pm 2.1 \times 10^{-3}$ $cm^2/V \cdot s$ (18 devices) and as high as 1.2×10^{-2} $cm^2/V \cdot s$, representing a 2 order of magnitude improvement in mobility compared to devices having as-evaporated HBC films. While the best of our TFTs exhibited mobilities that are still lower than the champion devices today, the 2 order of magnitude span in mobility observed in our HBC TFTs underscores the importance of active layer film structure and implicates the criticality in being able to prescribe it accordingly. The on/off ratio of these devices correspondingly increased to 10^3. Interestingly, the threshold voltage of these devices increased to $V_T = -42 \pm 2$ V compared to those of thermally annealed devices. While the origin of this increase in threshold voltage is unclear, we believe that the insulating oligomers on the surface of HBC in PDMS-treated devices are responsible for increasing the bias necessary to turn on the devices. Further corroborating this hypothesis is the fact that the contact resistance of the PDMS-treated devices is consistently higher than those of devices that have undergone other post-deposition treatments, as evidence in the superlinear characteristics in the linear regime the output curves shown in Figure S5d.

To elucidate this processing structure−function relationship that describes HBC TFTs, we quantified the preferential molecular orientation of HBC films in terms of the Hermans' orientation function analyzed about the (100) reflection, f_{100}:[28]

$$f_{100} = \frac{1}{2}(3\langle \cos^2\Phi_{100}\rangle - 1) \quad (2)$$

where

$$\langle \cos^2\Phi_{100}\rangle = \frac{\int_0^{\pi/2} I(\Phi)\sin\Phi \cos^2\Phi}{\int_0^{\pi/2} I(\Phi)\sin\Phi} \quad (3)$$

and Φ is the azimuthal angle; $I(\Phi)$ is the intensity of the (100) reflection as a function of the azimuthal angle. Accordingly, f_{100} can range from 1 to −0.5 wherein $f_{100} = 1$ indicates complete alignment of the (100) plane parallel to the substrate, or equivalently, an edge-on orientation of HBC; $f_{100} = -0.5$ indicates complete alignment of the (100) plane normal to the substrate; that is, HBC adopts a face-on orientation; and $f_{100} = 0$ indicates no preferential alignment of the (100) plane so HBC crystals are randomly oriented (see Supporting Information for details). Per eqs 2 and 3, we obtain f_{100} of −0.06, 0.04, and 0.87 for hexanes-vapor-annealed, thermally annealed, and PDMS-treated HBC films, respectively. Both the hexanes-vapor and thermally annealed films have f_{100} values near 0, implying that they exhibit only slight preferential orientation. However, the negative value of f_{100} for the hexanes-vapor-treated film indicates a slight preference for face-on orientation, whereas the slight positive value of f_{100} for the thermally annealed film indicates a slight preference for edge-on orientation. That f_{100} is 0.87 for the PDMS-treated film indicates that the film is highly oriented with HBC preferentially edge-on. Figure 4b plots the mobility extracted from these thin-film transistors as a function of the Herman's orientation function. These results show that the mobility of devices comprising crystalline HBC is positively correlated with the degree of edge-on orientation. Though this positive correlation between mobility and the degree of edge-on orientation is expected given what is known about charge transport in conjugated small molecules, these results stress the necessity for controlling the structure since small changes in the distribution of molecular orientations in films can impact the mobility of devices by several orders of magnitude.[6,29,30]

That we are able to prescribe the preferential molecular orientation in HBC active layers solely stems from the fact that as-evaporated HBC is disordered. Subsequent post-deposition processing allows the manipulation of the subtle competition between molecule−molecule and molecule−solvent interactions. The ability to access the rich phase space of structures is doubtlessly molecule-specific, but we have demonstrated comparable tunability in structure with seven other HBC derivatives. In materials systems besides HBCs, we have recently demonstrated the ability to alter in-plane crystal orientation of TES ADT by prepatterning the underlying substrate to have regions of different surface energies.[13] It is the subtle manipulation of molecule−substrate and molecule−molecule interactions during post-deposition crystallization of TES ADT that has afforded us structural tunability in this case.

Returning to the optical micrographs in Figure 1, we note interesting correlations between the preferential orientation of HBC at the molecular level and the structuring of spherulites on macroscopic length scales. In the case of PDMS-crystallized HBC, its spherulites resemble those of TES ADT.[22−24] We believe this similarity in the spherulitic texture between PDMS-crystallized HBC and solvent-vapor-annealed TES ADT stems from comparable molecular orientation at the molecular level as both compounds are preferentially oriented with their π-planes normal to the substrate.[23] Given the growth habit of TES ADT spherulites, we thus speculate that HBC, like TES ADT, crystallizes the fastest along its π-stacking direction, corresponding to the radial growth direction of spherulites. On the contrary, thermally and hexanes-vapor-annealed HBC films sample a broad distribution of molecular orientation, which

frustrates macroscopic spherulite growth and yields the complex textures observed in Figure 1c,d.

CONCLUSIONS

We have demonstrated the ability to tune the molecular orientation of HBC thin films deposited on a common substrate through post-deposition processing without further variation in molecular parameters or surface treatment. Variation in the molecular orientation of HBC is afforded by our ability to tune the subtle interplay between competing molecule−molecule and molecule−solvent interactions with these different post-deposition treatments.[31] Modeling is currently underway to elucidate the mechanistic origins of such tunability over the preferential orientation of HBC thin films. A greater understanding over the molecular-scale forces at play will allow for further decoupling of structural development from organic semiconductor deposition. Our findings suggest that, contrary to general belief, as-deposited organic semiconductor thin films exhibiting limited short-range order are not necessarily less desirable as they present an opportunity to subsequently dictate structural ordering through the delicate control over molecule−substrate, molecule−molecule, and molecule−solvent interactions.

METHODS

Substrate Preparation. Si(100) with thermally grown 300 nm SiO_2, purchased from Process Specialties, Inc., was used as substrates for both GIXD studies and for thin-film transistor measurements. The substrates were sonicated in acetone, IPA, and deionized water and dried with nitrogen. After cleaning, HMDS was deposited at 150 °C under at 2−4 Torr in an HMDS deposition chamber.

HBC Film Deposition. HBC, whose synthesis had been previously described elsewhere,[32,33] was thermally evaporated at 0.1−1 Å/s and 1×10^{-6} mbar atop HMDS-treated SiO_2/Si substrates to form continuous thin films *ca.* 120 nm thick. To rule out thickness effects, we maintained a constant thickness of 120 nm for all HBC films examined in this study.

Hexanes-Vapor Annealing. HBC films were placed in a covered Petri dish in air at room temperature in the presence of a reservoir of 10 mL of hexanes for 4 h. Despite being only sparingly soluble in hexanes, HBC crystallizes as the films are exposed to the solvent. Similar solvent-vapor annealing of an insoluble molecular semiconductor was demonstrated by Amassian and co-workers with pentacene and acetone.[12] Within 30 min of exposing HBC films to hexanes vapor, the films exhibit substantial crystallinity. Crystallization continues, and we observe improvements in birefringence upon extended exposures; GIXD confirms complete crystallization after 4 h of exposure to hexanes vapor. A myriad of solvents are applicable in this process. We chose hexanes because this solvent yields the same polymorph on HBC crystallization as when the as-evaporated films are subjected to thermal annealing and physical contact with PDMS. Further, the crystallization time scales during hexanes-vapor annealing are convenient so we can monitor this process optically *in situ*.

Thermal Annealing. Films were annealed at 240 °C on a hot plate until the film is completely crystallized (30 min in air). Crystallizing HBC can be accomplished by thermally annealing films at temperatures ranging from 215 to 255 °C; we chose 240 °C as crystallization at this temperature occurs on a time scale that we can monitor *in situ*. At these temperatures, HBC undergoes cold crystallization not unlike that commonly observed in semiflexible polymers, like poly(ethylene terephthalate).[34]

PDMS Preparation and Crystallization. Cross-linked PDMS elastomeric stamps were prepared using a Sylard 184 elastomer kit from Dow Corning. The elastomer base and curing agents were mixed in a 10:1 weight ratio. The mixture was deaerated and cured at 70 °C for 12−18 h before rectangular stamps were cut to size and contacted against HBC films for 12−24 h for crystallization to begin. The films subsequently crystallized over 1 to 3 weeks in air. Leaving PDMS atop HBC films for prolonged periods after crystallization has begun is undesirable as the HBC crystals tend to peel off when PDMS is removed.

GIXD Studies. GIXD experiments were conducted at the G1 station (10.0 ± 0.08 keV) of the Cornell High Energy Synchrotron Source. The beam was selected to be 0.05 mm tall and 1 mm wide. The width of the samples was 0.5 cm; this smaller sample width was chosen to reduce geometric smearing of peaks on the detector. The beam energy was selected with synthetic multilayer optics (W/B4C, 23.6 Å *d*-spacing). The X-ray beam was aligned above the film's critical angle and below the substrate's, at a 0.17° incident angle with the substrate. Scattered intensity was collected with a two-dimensional CCD detector, positioned 97.8 mm from the sample. All GIXD images have been background subtracted, and polarization and absorption corrections were applied, though these corrections were small.

NEXAFS Studies. NEXAFS experiments were carried out at the NIST/DOW soft X-ray materials characterization facility at beamline U7A at the National Synchrotron Light Source at Brookhaven National Laboratories. Partial electron yield (PEY) and fluorescent yield (FY) NEXAFS spectra were acquired simultaneously at the carbon K-edge. The spectra were normalized by the corresponding incident beam intensity and then subsequently pre- and post-edge normalized.[35−39] Details of analysis may be found in the Supporting Information.

Transistors. Top-contact (Au), bottom-gate (Si) thin-film transistors with an HMDS-treated 300 nm silicon dioxide dielectric layer were fabricated with 120 nm thick HBC thin films (same as in GIXD studies; see Substrate Preparation and HBC Film Deposition above for details). Next, 60 nm of Au was thermally evaporated through a stencil mask to produce source and drain contacts, defining active channels that were 2000 μm in width and 100 μm in length. Transistors were tested under nitrogen using an Agilent 4155C semiconductor parameter analyzer. Threshold voltages were calculated as the extrapolated zero point of the transfer curves in the saturated regime. On/off current ratios were calculated by taking the ratio of I_{DS} at $V_G = -100$ V (on) and 0 V (off) from output curves when V_{DS} was at −100 V.

Conflict of Interest: The authors declare no competing financial interest.

Acknowledgment. This work was supported by the NSF MRSEC program through the Princeton Center for Complex Materials (DMR-0819860). GIXD experiments were conducted at CHESS, which is supported by NSF and NIH/NIGMS under award DMR-0936384. A.M.H. and S.S.L. thank the National Defense Science and Engineering Graduate Fellowships. A.M.H. was also partially supported by an NSF IGERT Fellowship (0903661). We also thank Rich Fiorillo for his technical support.

Supporting Information Available: Details of NEXAFS analysis; details of Herman's orientation function analysis of GIXD data; optical micrograph of PDMS-patterned crystalline HBC film; AFM micrographs of crystallized thin films; representative output characteristics of TFTs. This material is available free of charge *via* the Internet at http://pubs.acs.org.

REFERENCES AND NOTES

1. Sundar, V. C.; Zaumseil, J.; Podzorov, V.; Menard, E.; Willett, R. L.; Someya, T.; Gershenson, M. E.; Rogers, J. A. Elastomeric Transistor Stamps: Reversible Probing of Charge Transport in Organic Crystals. *Science* **2004**, *303*, 1644–1646.
2. Lee, J. Y.; Roth, S.; Park, Y. W. Anisotropic Field Effect Mobility in Single Crystal Pentacene. *Appl. Phys. Lett.* **2006**, *88*, 252106.

3. Salleo, A.; Kline, R. J.; DeLongchamp, D. M.; Chabinyc, M. L. Microstructural Characterization and Charge Transport in Thin Films of Conjugated Polymers. *Adv. Mater.* **2010**, *22*, 3812–3838.
4. Sirringhaus, H.; Brown, P. J.; Friend, R. H.; Nielsen, M. M.; Bechgaard, K.; Langeveld-Voss, B. M. W.; Spiering, A. J. H.; Janssen, R. A. J.; Meijer, E. W.; Herwig, P.; *et al.* Two-Dimensional Charge Transport in Self-Organized, High-Mobility Conjugated Polymers. *Nature* **1999**, *401*, 685–688.
5. Gundlach, D. J.; Lin, Y. Y.; Jackson, T. N.; Nelson, S. F.; Schlom, D. G. Pentacene Organic Thin-Film Transistors—Molecular Ordering and Mobility. *IEEE Electron Device Lett.* **1997**, *18*, 87–89.
6. Kim, D. H.; Park, Y. D.; Jang, Y.; Yang, H.; Kim, Y. H.; Han, J. I.; Moon, D. G.; Park, S.; Chang, T.; Chang, C.; *et al.* Enhancement of Field-Effect Mobility Due to Surface-Mediated Molecular Ordering in Regioregular Polythiophene Thin Film Transistors. *Adv. Funct. Mater.* **2005**, *15*, 77–82.
7. Hu, W. S.; Tao, Y. T.; Hsu, Y. J.; Wei, D. H.; Wu, Y. S. Molecular Orientation of Evaporated Pentacene Films on Gold: Alignment Effect of Self-Assembled Monolayer. *Langmuir* **2005**, *21*, 2260–2266.
8. Verreet, B.; Muller, R.; Rand, B. P.; Vasseur, K.; Heremans, P. Structural Templating of Chloro-aluminum Phthalocyanine Layers for Planar and Bulk Heterojunction Organic Solar Cells. *Org. Electron.* **2011**, *12*, 2131–2139.
9. Kim, J. S.; Park, Y.; Lee, D. Y.; Lee, J. H.; Park, J. H.; Kim, J. K.; Cho, K. Poly(3-hexylthiophene) Nanorods with Aligned Chain Orientation for Organic Photovoltaics. *Adv. Funct. Mater.* **2010**, *20*, 540–545.
10. De Luca, G.; Pisula, W.; Credgington, D.; Treossi, E.; Fenwick, O.; Lazzerini, G. M.; Dabirian, R.; Orgiu, E.; Liscio, A.; Palermo, V.; *et al.* Non-conventional Processing and Post-processing Methods for the Nanostructuring of Conjugated Materials for Organic Electronics. *Adv. Funct. Mater.* **2011**, *21*, 1279–1295.
11. Palermo, V.; Samorì, P. Molecular Self-Assembly Across Multiple Length Scales. *Angew. Chem., Int. Ed.* **2007**, *46*, 4428–4432.
12. Amassian, A.; Pozdin, V. A.; Li, R.; Smilgies, D.-M.; Malliaras, G. G. Solvent Vapor Annealing of an Insoluble Molecular Semiconductor. *J. Mater. Chem.* **2010**, *20*, 2623–2629.
13. Lee, S. S.; Tang, S. B.; Smilgies, D.-M.; Woll, A. R.; Loth, M. A.; Mativetsky, J. M.; Anthony, J. E.; Loo, Y.-L. Guiding Crystallization around Bends and Sharp Corners. *Adv. Mater.* **2012**, *24*, 2692–2698.
14. Fabiano, S.; Wang, H.; Piliego, C.; Jaye, C.; Fischer, D. A.; Chen, Z.; Pignataro, B.; Facchetti, A.; Loo, Y.-L.; Loi, M. A. Supramolecular Order of Solution-Processed Perylenediimide Thin Films: High-Performance Small-Channel n-Type Organic Transistors. *Adv. Funct. Mater.* **2011**, *21*, 4479–4486.
15. Tremblay, N. J.; Gorodetsky, A. A.; Cox, M. P.; Schiros, T.; Kim, B.; Steiner, R.; Bullard, Z.; Sattler, A.; So, W. Y.; Itoh, Y.; *et al.* Photovoltaic Universal Joints: Ball-and-Socket Interfaces in Molecular Photovoltaic Cells. *ChemPhysChem* **2010**, *11*, 799–803.
16. Sygula, A.; Fronczek, F. R.; Sygula, R.; Rabideau, P. W.; Olmstead, M. M. A Double Concave Hydrocarbon Buckycatcher. *J. Am. Chem. Soc.* **2007**, *129*, 3842–2843.
17. Blasini, D. R.; Rivnay, J.; Smilgies, D. M.; Slinker, J. D.; Flores-Torres, S.; Abruna, H. D.; Malliaras, G. G. Observation of Intermediate-Range Order in a Nominally Amorphous Molecular Semiconductor Film. *J. Mater. Chem.* **2007**, *17*, 1458–1461.
18. Proehl, H.; Toerker, M.; Sellam, F.; Fritz, T.; Leo, K.; Simpson, C.; Mullen, K. Comparison of Ultraviolet Photoelectron Spectroscopy and Scanning Tunneling Spectroscopy Measurements on Highly Ordered Ultrathin Films of Hexa-perihexabenzocoronene on Au(111). *Phys. Rev. B* **2001**, *63*, 205409.
19. Xiao, S. X.; Myers, M.; Miao, Q.; Sanaur, S.; Pang, K. L.; Steigerwald, M. L.; Nuckolls, C. Molecular Wires from Contorted Aromatic Compounds. *Angew. Chem., Int. Ed.* **2005**, *44*, 7390–7394.
20. Cohen, Y. S.; Xiao, S.; Steigerwald, M. L.; Nuckolls, C.; Kagan, C. R. Enforced One-Dimensional Photoconductivity in Core-Cladding Hexabenzocoronenes. *Nano Lett.* **2006**, *6*, 2838–2841.
21. Clar, E.; Stephen, J. F. Synthesis of 1-2,3-4,5-6,7-8,9-10,11-12-Hexabenzocoronene. *Tetrahedron* **1965**, *21*, 467–470.
22. Dickey, K. C.; Anthony, J. E.; Loo, Y.-L. Improving Organic Thin-Film Transistor Performance through Solvent-Vapor Annealing of Solution-Processable Triethylsilylethynyl Anthradithiophene. *Adv. Mater.* **2006**, *18*, 1721–1726.
23. Lee, S. S.; Kim, C. S.; Gomez, E. D.; Purushothaman, B.; Toney, M. F.; Wang, C.; Hexemer, A.; Anthony, J. E.; Loo, Y.-L. Controlling Nucleation and Crystallization in Solution-Processed Organic Semiconductors for Thin-Film Transistors. *Adv. Mater.* **2009**, *21*, 3605–3609.
24. Lee, S. S.; Loth, M. A.; Anthony, J. E.; Loo, Y.-L. Orientation-Independent Charge Transport in Single Spherulites from Solution-Processed Organic Semiconductors. *J. Am. Chem. Soc.* **2012**, *134*, 5436–5439.
25. Shtukenberg, A. G.; Punin, Y. O.; Gunn, E.; Kahr, B. Spherulites. *Chem. Rev.* **2012**, *112*, 1805–1838.
26. Chu, J. H.; Rangarajan, P.; Adams, J. L.; Register, R. A. Morphologies of Strongly Segregated Polystrene-Poly(dimethylsiloxane) Diblock Copolymers. *Polymer* **1995**, *36*, 1569–1575.
27. Kim, Y.; Choulis, S. A.; Nelson, J.; Bradley, D. D. C.; Cook, S.; Durrant, J. R. Device Annealing Effect in Organic Solar Cells with Blends of Regioregular Poly(3-hexylthiophene) and Soluble Fullerene. *Appl. Phys. Lett.* **2005**, *86*, 063502.
28. Gedde, U. W. *Polymer Physics*, 1st ed.; Springer: Berlin, 1995; p 298.
29. Lee, S. S.; Loo, Y.-L. Structural Complexities in the Active Layers of Organic Electronics. *Annu. Rev. Chem. Biomol.* **2010**, *1*, 59–78.
30. Pisula, W.; Menon, A.; Stepputat, M.; Lieberwirth, I.; Kolb, U.; Tracz, A.; Sirringhaus, H.; Pakula, T.; Mullen, K. A Zone-Casting Technique for Device Fabrication of Field-Effect Transistors Based on Discotic Hexa-peri-hexabenzoeoronene. *Adv. Mater.* **2005**, *17*, 684–689.
31. Hurt, R.; Krammer, G.; Crawford, G.; Jian, K.; Rulison, C. Polyaromatic Assembly Mechanisms and Structure Selection in Carbon Materials. *Chem. Mater.* **2002**, *14*, 4558–4565.
32. Plunkett, K. N.; Godula, K.; Nuckolls, C.; Tremblay, N.; Whalley, A. C.; Xiao, S. Expeditious Synthesis of Contorted Hexabenzocoronenes. *Org. Lett.* **2009**, *11*, 2225–2228.
33. Loo, Y.-L.; Hiszpanski, A. M.; Kim, B.; Wei, S.; Chiu, C.-Y.; Steigerwald, M. L.; Nuckolls, C. Unusual Molecular Conformations in Fluorinated, Contorted Hexabenzocoronenes. *Org. Lett.* **2010**, *12*, 4840–4843.
34. Liu, T.; Petermann, J. Multiple Melting Behavior in Isothermally Cold-Crystallized Isotactic Polystyrene. *Polymer* **2001**, *42*, 6453–6461.
35. Stohr, J. *NEXAFS Spectroscopy*; Springer: Berlin, 1992.
36. Krapchetov, D. A.; Ma, H.; Jen, A. K. Y.; Fischer, D. A.; Loo, Y.-L. Solvent-Dependent Assembly of Terphenyl- and Quaterphenyldithiol on Gold and Gallium Arsenide. *Langmuir* **2005**, *21*, 5887–5893.
37. Krapchetov, D. A.; Ma, H.; Jen, A. K. Y.; Fischer, D. A.; Loo, Y.-L. Deprotecting Thioacetyl-Terminated Terphenyldithiol for Assembly on Gallium Arsenide. *Langmuir* **2008**, *24*, 851–856.
38. Sohn, K. E.; Dimitriou, M. D.; Genzer, J.; Fischer, D. A.; Hawker, C. J.; Kramer, E. J. Determination of the Electron Escape Depth for NEXAFS Spectroscopy. *Langmuir* **2009**, *25*, 6341–6348.
39. Wang, H.; Gomez, E. D.; Kim, J.; Guan, Z.; Jaye, C.; Fischer, D. A.; Kahn, A.; Loo, Y.-L. Device Characteristics of Bulk-Heterojunction Polymer Solar Cells are Independent of Interfacial Segregation of Active Layers. *Chem. Mater.* **2011**, *23*, 2020–2023.